



## UvA-DARE (Digital Academic Repository)

### Searching for the spectral depolarisation of ASKAP one-off FRB sources

Uttarkar, P.A.; Shannon, R.M.; Gourджи, K.; Deller, A.T.; Day, C.K.; Bhandari, S.

**DOI**

[10.1093/MNRAS/STAD3437](https://doi.org/10.1093/MNRAS/STAD3437)

**Publication date**

2024

**Document Version**

Final published version

**Published in**

Monthly Notices of the Royal Astronomical Society

**License**

CC BY

[Link to publication](#)

**Citation for published version (APA):**

Uttarkar, P. A., Shannon, R. M., Gourджи, K., Deller, A. T., Day, C. K., & Bhandari, S. (2024). Searching for the spectral depolarisation of ASKAP one-off FRB sources. *Monthly Notices of the Royal Astronomical Society*, 527(2), 4285-4296. <https://doi.org/10.1093/MNRAS/STAD3437>







**General rights**

It is not permitted to download or to forward/distribute the text or part of it without the consent of the author(s) and/or copyright holder(s), other than for strictly personal, individual use, unless the work is under an open content license (like Creative Commons).

**Disclaimer/Complaints regulations**

If you believe that digital publication of certain material infringes any of your rights or (privacy) interests, please let the Library know, stating your reasons. In case of a legitimate complaint, the Library will make the material inaccessible and/or remove it from the website. Please Ask the Library: <https://uba.uva.nl/en/contact>, or a letter to: Library of the University of Amsterdam, Secretariat, Singel 425, 1012 WP Amsterdam, The Netherlands. You will be contacted as soon as possible.

# Searching for the spectral depolarization of ASKAP one-off FRB sources

Pavan A. Uttarkar <sup>1</sup>★, R. M. Shannon <sup>1</sup>★, K. Gourdji <sup>1</sup>★, A. T. Deller <sup>1</sup>, C. K. Day <sup>2</sup>  
and S. Bhandari <sup>3,4,5</sup>

<sup>1</sup>Centre for Astrophysics and Supercomputing, Swinburne University of Technology, Hawthorn, VIC 3122, Australia

<sup>2</sup>Department of Physics, McGill University, Montreal, Quebec H3A 2T8, Canada

<sup>3</sup>ASTRON, Netherlands Institute for Radio Astronomy, Oude Hoogeveensedijk 4, NL-7991 PD Dwingeloo, the Netherlands

<sup>4</sup>Joint institute for VLBI ERIC, Oude Hoogeveensedijk 4, NL-7991 PD Dwingeloo, the Netherlands

<sup>5</sup>Anton Pannekoek Institute for Astronomy, University of Amsterdam, Science Park 904, NL-1098 XH, Amsterdam, the Netherlands

Accepted 2023 November 2. Received 2023 October 20; in original form 2023 March 7

## ABSTRACT

Fast Radio Bursts (FRBs) are extragalactic transients of (sub-)millisecond duration that show wide-ranging spectral, temporal, and polarimetric properties. The polarimetric analysis of FRBs can be used to probe intervening media, study the emission mechanism, and test possible progenitor models. In particular, low-frequency depolarization of FRBs can identify dense, turbulent, magnetized, ionized plasma thought to be near the FRB progenitor. An ensemble of repeating FRBs has shown low-frequency depolarization. The depolarization is quantified by the parameter  $\sigma_{\text{RM}}$ , which correlates with proxies for both the turbulence and mean magnetic field strength of the putative plasma. However, while many non-repeating FRBs show comparable scattering (and hence inferred turbulence) to repeating FRBs, it is unclear whether their surrounding environments are comparable to those of repeating FRBs. To test this, we analyse the spectro-polarimetric properties of five one-off FRBs and one repeating FRB, detected and localized by the Australian Square Kilometer Array Pathfinder. We search for evidence of depolarization due to  $\sigma_{\text{RM}}$  and consider models where the depolarization is intrinsic to the source. We find no evidence (for or against) the sample showing spectral depolarization. Under the assumption that FRBs have multipath propagation-induced depolarization, the correlation between our constraint on  $\sigma_{\text{RM}}$  and RM is consistent with repeating FRBs only if the values of  $\sigma_{\text{RM}}$  are much smaller than our upper limits. Additionally, the correlation between the constraints on  $\sigma_{\text{RM}}$  and  $\tau_s$  is inconsistent with repeating FRBs. The observations provide further evidence for differences in the typical environments and sources of one-off and repeating FRBs.

**Key words:** polarization – methods: data analysis – fast radio bursts.

## 1 INTRODUCTION

Fast Radio Bursts (FRBs) are (sub-)millisecond duration transients of extragalactic origin. The first FRB was discovered in archival Parkes data (Lorimer et al. 2007). Since the first reported burst, there have been more than 600 FRB detections published (e.g. Xu et al. 2023).

Of those, only  $\sim 65$  FRBs are currently known to repeat, with FRB 20121102A and FRB 20180916B showing periodic activity (Chime/FRB Collaboration et al. 2020; Rajwade et al. 2020). Whether all FRBs can be eventually observed to repeat is unclear (Caleb et al. 2019). FRBs have been observed over a wide range of frequencies, in bands from 110–180 MHz (Pleunis et al. 2021a) to 4–8 GHz (Gajjar et al. 2018). While FRBs were initially speculated to be associated with cataclysmic events (Thornton et al. 2013), this thinking had to be updated after the discovery of the first repeating FRB (Spitler et al. 2016). An early analysis

of four bursts detected from the High Time Resolution Universe (HTRU) Survey using the Parkes 64-m radio telescope suggested the FRB volumetric occurrence rate above a fluence of 3 Jy ms to be  $\sim 10^4 \text{ sky}^{-1} \text{ day}^{-1}$  (Thornton et al. 2013). An analysis by Ravi (2019) considering the CHIME/FRB detections shows the FRB volumetric occurrence rate to be higher than the event rate for cataclysmic source classes such as supernova explosions or neutron star mergers, concluding that a significant fraction of FRBs could be repeating sources.

In addition to representing a new astrophysical phenomenon of unknown origin, FRBs promise to be useful as cosmological probes. The interferometric localizations of one-off FRB sources to their host galaxies (e.g. Bannister et al. 2019; Prochaska et al. 2019; Cho et al. 2020; Day et al. 2020) have enabled the measurement of the cosmic baryon density in the low-redshift Universe (Macquart et al. 2020). Additionally, localized FRB sources from the Australian Square Kilometer Array Pathfinder (ASKAP), along with Parkes-detected FRBs, have provided an independent measurement of Hubble’s constant (James et al. 2022). In the future, a more precise measurement with an uncertainty of  $\pm 2.5 \text{ km s}^{-1} \text{ Mpc}^{-1}$  may be possible with a larger sample of localized FRBs (James et al. 2022).

\* E-mail: [puttarkar@swin.edu.au](mailto:puttarkar@swin.edu.au) (PAU); [rmshannon@swin.edu.au](mailto:rmshannon@swin.edu.au) (RMS); [kgourdji@swin.edu.au](mailto:kgourdji@swin.edu.au) (KG)

Repeating and (apparently) non-repeating FRBs can show different characteristic spectral and temporal properties. This includes linear frequency drift of intra-burst emission with time ('sawtooth' structure) observed in repeating FRBs (e.g. CHIME/FRB Collaboration et al. 2019; Hessels et al. 2019). There is also evidence that the bursts from repeating FRBs are generally of longer duration than non-repeating FRBs and that repeating FRBs show band-limited structure (e.g. Gourdji et al. 2019; CHIME/FRB Collaboration et al. 2021; Kumar et al. 2021; Pleunis et al. 2021b). Some repeating FRBs also exhibit an increase in fractional bandwidth with frequency (Bethapudi et al. 2022).

A small fraction of repeating FRBs also exhibits drastic variations in spectro-polarimetric characteristics, such as the extremely narrow-banded burst observed from the repeating source FRB 20190711A (Kumar et al. 2021). Initial 5-GHz polarimetric studies of the first known repeating FRB 20121102A reported a high degree of linear polarization ( $\sim 100$  per cent) along with a flat polarization position angle (PPA) (Michilli et al. 2018). However, subsequent reported observations of repeaters, such as FRB 20201124A (Kumar et al. 2022) and FRB 20180301A (Luo et al. 2020) indicate more diverse polarimetric behaviour, with the PPA varying across the burst envelope. In comparison, the sample of non-repeaters with polarimetric information displays a variety of polarization fractions, with the majority showing high degrees of linear polarization ( $> 90$  per cent; e.g. Cho et al. 2020; Day et al. 2020). Some non-repeating FRBs also show a relatively high degree of circular polarization ( $\sim 5$  per cent; e.g. Bhandari et al. 2020; Day et al. 2020), while others appear to exhibit sub-burst to sub-burst variation in the polarization fraction along with varying Rotation Measures (RM; Cho et al. 2020; Day et al. 2020).

Repeating and non-repeating FRBs also show differences in RM, with some repeating FRBs showing extremely large RM magnitudes, such as the first detected repeater FRB 20121102A (Michilli et al. 2018), which has a measured RM of  $\sim 10^5 \text{ rad m}^{-2}$ . This FRB also shows a secular decline in RM ( $\sim 15$  per cent  $\text{yr}^{-1}$ ) as well as short-term variations of up to  $\sim 1$  per cent  $\text{week}^{-1}$  (Michilli et al. 2018; Hilmarsson et al. 2021). FRB 20190520B displays an even larger RM variation from  $10^4$  to  $\sim -1.6 \times 10^4 \text{ rad m}^{-2}$  over approximately six months suggesting a reversal in the magnetic field. Such variation in RM shown in FRBs 20190520B and 20121102A has been interpreted as arising from a complex turbulent circumburst magnetoionic environment (Anna-Thomas et al. 2022). The RM magnitude and variations can be used to develop models for the surrounding environment. For instance, the detected reversal in the magnetic field reported by Anna-Thomas et al. (2022) was speculated to be caused by the presence of a highly magnetized stellar or black-hole companion. In contrast, non-repeating FRBs have been observed to have less extreme rotation measures (less than a few hundred  $\text{rad m}^{-2}$ ), consistent with passage through Milky-Way-like columns in the interstellar medium (ISM)<sup>1</sup> (Mannings et al. 2022).

Another potential diagnostic of FRB environments arises from the spectral depolarization of burst emission. Early observations showed that the linear polarization fraction of the Crab nebula was lower than expected and decreased at lower frequencies (Gardner & Whiteoak 1963). The variation of the linear polarization fraction as a function of frequency was explained by Burn (1966) to be due to the random orientation of the magnetic field, leading to Faraday rotation in its shell. The strength of the effect is quantified by the scatter

<sup>1</sup>For obvious reasons, long-term rotation measure variations have not been observed in non-repeating FRBs.

RM measure,  $\sigma_{\text{RM}}$ . Similar depolarization behaviour was recently reported by Feng et al. (2022) in repeating FRBs. Using observations from several different telescopes across a frequency range of 115 to 4600 MHz, their sample also shows a clear trend of decreasing linear polarization fraction with decreasing frequency, with reported  $\sigma_{\text{RM}}$  from 0.12 to 218  $\text{rad m}^{-2}$ . The depolarization reported was quantified using multipath propagation due to the foreground scattering screen, which includes the host galaxy and Milky Way. This is different from the depolarization that has been seen in extended sources, which can be explained due to the differential RM in the source itself (Burn 1966). A correlation was also reported between the  $\sigma_{\text{RM}}$ , RM and scatter-broadening time  $\tau_s$  (Feng et al. 2022). This inferred depolarization behaviour provides a diagnostic of intervening media and can be used to constrain possible progenitor and emission mechanism models. Notably, the two sources with the highest values of  $\sigma_{\text{RM}}$ , FRBs 20121102A ( $30.9 \pm 0.4 \text{ rad m}^{-2}$ ; Chatterjee et al. 2017; Feng et al. 2022) and 20190520B ( $218 \pm 10.2 \text{ rad m}^{-2}$ ; Niu et al. 2022; Feng et al. 2022), are associated with persistent radio sources.

It is unclear if spectral depolarization is present in non-repeating FRBs. Measuring this effect is challenging in non-repeating FRBs as the search data streams are constrained to modest observing bandwidths and low time and frequency resolution. These streams might also be affected by intra-channel depolarization and dispersion smearing. Some search systems include voltage buffers that provide higher time and spectral resolution, but these are usually still bandwidth limited. An investigation of the effects of depolarization among non-repeating FRBs would provide insight into the dichotomy of repeating and non-repeating FRBs and potentially serve as a diagnostic of the properties of their respective circumburst media.

The Commensal Real-Time ASKAP Fast Transient (CRAFT) survey system currently utilizes two parallel data streams: a low-time resolution stream in Stokes I to search for FRBs and a  $\sim 3.1$ -s voltage buffer, which is triggered if an FRB candidate is detected. These voltages, saved for individual antennas, are then used for interferometric localization and to produce high-time resolution data products (e.g. Bannister et al. 2019; Cho et al. 2020; Day et al. 2020; Macquart et al. 2020). In this paper, we study ASKAP reported FRBs, among which FRB 20180924B (Bannister et al. 2019), FRB 20190102C, FRB 20190608B, FRB 20190611B and FRB 20191001A are one-off FRBs (Bhandari et al. 2020; Day et al. 2020; Macquart et al. 2020). We also examine the repeating source FRB 20190711A (Day et al. 2020). We search for depolarization in individual sub-bursts as well as the integrated burst for all FRBs. We also compare three different depolarization models using the set of six FRBs to investigate apparent correlations between  $\sigma_{\text{RM}}$ , RM, and  $\tau_s$ . We describe the data selection and models for depolarization in Section 2 and the results in Section 3. We conclude with a discussion of the potential models and implications for the populations of repeaters and non-repeaters in Section 4.

## 2 METHODOLOGY

### 2.1 Data selection and description

The polarimetric analysis is performed on a set of five localized ASKAP one-off FRB sources and one localized repeating ASKAP FRB source. These FRB data sets were detected by the CRAFT real-time detection system and were first reported in Bannister et al. (2019), Bhandari et al. (2020), and Macquart et al. (2020). After the bursts were detected, dual-polarization voltage buffers were downloaded from individual antennas. These voltage buffers were

then calibrated for flux, phase, and polarization and then coherently analysed to study burst spectro-temporal polarimetry (Day et al. 2020). For FRBs 20180924B, 20190608B, 20190102C, 20190611B, and 20190711A, we used image domain, de-dispersed data sets described in Day et al. (2020). For FRB 20191001A, we used the High Time Resolution (HTR) de-dispersed complex voltages presented in Bhandari et al. (2020), using methods described in Cho et al. (2020).

The data used to analyse FRBs 20180924B, 20190102C, 20190608B, 20190611B, and 20190711A have a recorded bandwidth of 336 MHz, with  $\sim 4$  MHz of channel resolution each, at a centre frequency of 1272 MHz. The data used to analyse FRBs 20180924B and 20191001A have central frequencies of 1320 and 824 MHz, respectively. For FRB 20191001A, there was only 144 MHz of recorded bandwidth because of the latency in the detection pipeline and short (3.1 s) duration of the voltage buffer, which caused the FRB to be overwritten in the high frequency part of the band.

The dynamic Stokes-I spectra, polarization position angle (PPA), and the RM-corrected polarization profile of the bursts are shown in Fig. 1. Among our sample, FRBs 20190611B, 20190711A, and 20190102C shows distinct sub-bursts. FRB 20190102C has one faint sub-burst before the main pulse that shows a significantly different polarization fraction relative to the main burst but with a similar RM (Day et al. 2020). The repeating source FRB 20190711A shows three characteristic sub-bursts, all having similar RMs and showing complex pulse morphology (Day et al. 2020). With the exception of FRB 20191001A, all FRBs have a high fractional linear polarization ( $> 90$  per cent; Bhandari et al. 2020; Day et al. 2020).

## 2.2 Measuring linear polarization fraction

Faraday rotation is the frequency-dependent rotation of plane of linear polarization induced by the magnetic field component parallel to the line of sight of the observer to the intervening cold-magnetized plasma. The magnitude of the effect is quantified by the rotation measure (RM). The change in the PPA is given by

$$\text{PPA} = \text{RM}_{\text{obs}}(\lambda^2 - \lambda_0^2), \quad (1)$$

where  $\lambda$  is the wavelength,  $\lambda_0$  is the wavelength of the centre frequency of the observing band, and  $\text{RM}_{\text{obs}}$  is defined to be

$$\text{RM}_{\text{obs}} = \frac{e^3}{2\pi m_e^2 c^4} \int_d^0 \frac{n_e B_{\parallel}}{(1+z)^2} dl, \quad (2)$$

where  $d$  is the distance to the source of emission,  $m_e$  is the electron mass,  $e$  is the charge of the electron,  $B_{\parallel}$  is the magnetic field parallel to the line of sight, and  $z$  is the redshift of the plasma. The individual Dispersion Measure (DM), RM, time, and frequency resolution of the bursts reported in Bhandari et al. (2020) and Day et al. (2020) are listed in Table 1. We calculate the fraction of linear polarization of individual sub-bursts and the integrated burst (integration across all the sub-bursts) from the polarization calibrated data set for our sample. (For a rigorous description of the analysis, refer Bhandari et al. (2020) and Day et al. (2020).)

To measure the linear polarization fraction of the bursts, we first de-rotate the calibrated spectra to account for burst RM:

$$\begin{aligned} U_{\text{cor}} &= -Q_{\text{cal}} \cos(2\phi) + U_{\text{cal}} \sin(2\phi), \\ Q_{\text{cor}} &= Q_{\text{cal}} \cos(2\phi) + U_{\text{cal}} \sin(2\phi), \end{aligned} \quad (3)$$

where  $Q_{\text{cal}}$  and  $U_{\text{cal}}$  are the polarization-calibrated spectra of individual bursts and  $\phi$  is the PPA. The de-rotation is conducted using the RMs from Table 1 for individual sub-bursts in the set of FRBs.

After this, further averaging in frequency is performed to increase the signal-to-noise ratio (S/N) in individual spectral measurements. We average each FRB and sub-burst differently to account for their varying S/N, as described in Section 2.3. The total linear polarization estimator  $L_{\text{cal}} = \sqrt{Q_{\text{cor}}^2 + U_{\text{cor}}^2}$  is a biased estimate due to the presence of noise, especially at low to intermediate S/N (Everett & Weisberg 2001). To obtain an unbiased estimate of the polarization fraction, de-biasing is performed, following equation (4), originally presented in Wardle & Kronberg (1974):

$$L_{\text{de-bias}} = \begin{cases} \sigma_1 \sqrt{\left(\frac{L_{\text{cal}}}{\sigma_1}\right)^2 - 1}, & \text{if } \frac{L_{\text{cal}}}{\sigma_1} \geq 1.57\beta \\ 0, & \text{otherwise,} \end{cases} \quad (4)$$

where  $L_{\text{cal}}$  is the linear polarization calculated from the calibrated Stokes-Q and Stokes-U spectra, and  $\sigma_1$  is the uncertainty in the Stokes-I spectrum. We follow the de-biasing method used in Everett & Weisberg (2001) and choose a higher threshold of  $\beta = 2$  for our analysis, to account for low S/N measurements, due to the band-limited structure in some of the bursts.

## 2.3 Bayesian modelling for match-filtering

To maximize the S/N in an individual Stokes spectrum, we use a match-filtering approach to average over the burst envelope. On average, the match filtering approach provides an improvement of  $\sim 49$  per cent in the polarized SNR, relative to a simple boxcar (i.e. non-weighted average). The improvement is more pronounced for FRBs 20180924B, 20190102C, 20190608B, 20190611B, and 20190711A, which have HTR image domain data sets, compared to FRB 20191001A, which has HTR beamformed data available. Using a Bayesian framework, we model the burst envelopes assuming either a Gaussian or a Gaussian convolved with an exponential if the burst shows evidence for scatter broadening.

In the case of a Gaussian pulse, we model the burst to be

$$W_{\text{pulse}}(t) = A \exp\left(-\frac{(t-t_0)^2}{2\sigma^2}\right), \quad (5)$$

where  $A$  is the amplitude of the pulse,  $t_0$  is the centre of the pulse and the pulse width (the full width at half-maximum) is  $2\sigma\sqrt{2\ln 2}$ .

In the case of a scatter-broadened pulse, we assume the pulse to be a Gaussian convolved with an exponential, pulse-broadening function (PBF),

$$\text{PBF}(t) = \begin{cases} \exp\left(-\frac{t}{\tau}\right) & \text{if } t > 0 \\ 0, & \text{otherwise,} \end{cases} \quad (6)$$

where  $\tau$  is the scattering time. The weights are calculated for a Gaussian and Gaussian convolved exponential functions as defined above. A weighted average is performed, with the weights estimated for individual time bins of the de-rotated Stokes spectrum at coarser frequency resolution. We average the RM corrected polarization spectra of FRBs to a frequency resolution listed in Table 1. The coarser frequency resolution of each FRB is non-identically averaged to account for the individual burst spectral extent (e.g. limited spectral extent of FRB 20190611B), and to have at least three frequency measurements for the integrated pulse.

We use exponentially convolved Gaussian models for FRBs 20180924B, 20190608B, and 20191001A. For FRBs 20190102C and 20190611B, Gaussian and exponentially convolved Gaussian models are used for different components. We do not fit any model for FRB 20190711A, due to its complex temporal structure. To fit



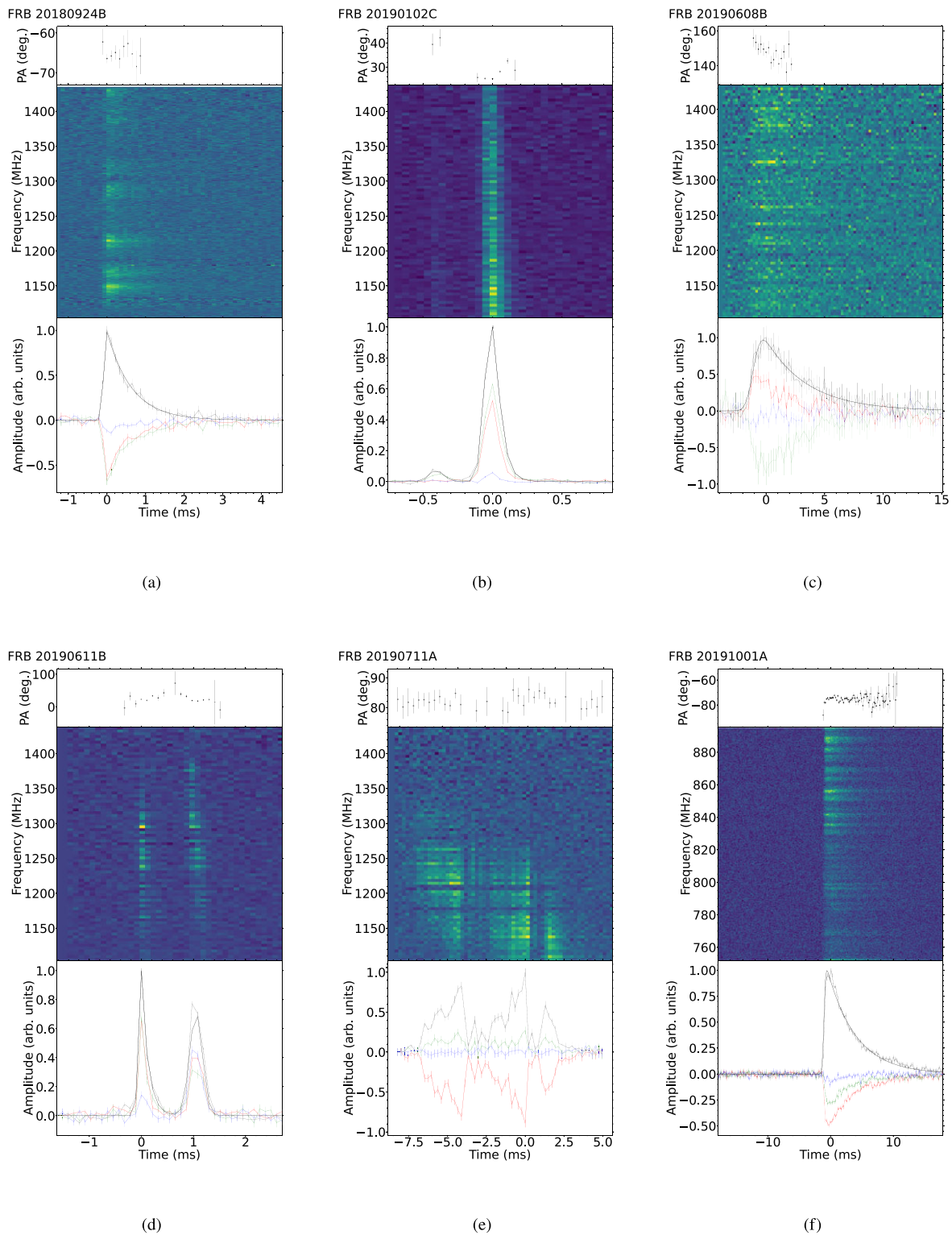


**Figure 1.** The PA angle, Stokes-I dynamic spectrum, and polarization profiles for each burst are shown in the top, middle, and bottom panels, respectively. Stokes-I, Q, U, and V are, respectively, shown in black, red, green, and blue dashed lines in the bottom panel. The match filter kernel is indicated by the black solid line for all the bursts in the bottom panel. We only show the PA angle for time bins with  $S/N > 5$  in Stokes-I. FRBs 20180924B, 20190102C, 20190608B, 20190611B, and 20190711A are shown with a spectral resolution of 4 MHz and temporal resolution of 0.108, 0.054, 0.261, 0.108, and 0.216 ms, respectively. We show FRB 20191001A with a spectral resolution of 0.5 MHz and a temporal resolution of 0.18 ms. We use a simple boxcar for FRB 20190711A. Hence, no match filter kernel is shown in its polarization profile.

**Table 1.** The table lists RM, DM, frequency resolution and time resolution for FRBs in our sample. For bursts with subcomponents, we list both the quantities derived from those and the entire burst. For FRBs 20180924B, 20190102C, 20190608B, 20190611B, and 20190711A, we list the time resolution from Day et al. (2020). The listed frequency resolution is the averaged frequency channel width after RM correction used for the model fit for model comparison.

TNS Name	Sub-burst	DM (pc cm <sup>-3</sup> )	Rotation measure (rad m <sup>-2</sup> )	Frequency resolution (MHz)	Time resolution (ms)
FRB 20180924B	–	362.2	22 ± 2	33.6	0.108
FRB 20190102C	–	364.538	−105 ± 1	28	0.054
	sub-burst 0	–	−128 ± 7	–	–
	sub-burst 1	–	−105 ± 1	–	–
FRB 20190608B	–	339.79	353 ± 2	67.2	0.261
FRB 20190611B	–	332.60	20 ± 4	33.6	0.108
	sub-burst 0	–	19 ± 4	–	–
	sub-burst 1	–	12 ± 2	–	–
FRB 20190711A	–	587.87	9 ± 2	56	0.216
	sub-burst 0	–	10 ± 4	–	–
	sub-burst 1	–	9 ± 3	–	–
	sub-burst 2	–	12 ± 6	–	–
FRB 20191001A	–	506.92	55.5 ± 9	14.4	0.18

these models, we use a Gaussian likelihood (and assume the noise in our data is Gaussian distributed):

$$L(P_i | P_M, \sigma) = \prod_i^{N_f} \frac{1}{\sqrt{2\pi\sigma^2}} \exp\left(-\frac{(P_i - P_{M,i})^2}{2\sigma^2}\right), \quad (7)$$

where  $P_i$  is the measured fractional polarization data in frequency channel  $i$ ,  $P_M$  is the modelled fractional linear polarization fraction, and  $\sigma$  is the standard deviation. We describe the models for linear polarization fraction  $P_M$  below. Parameter estimation is performed using the software package `bilby` (Ashton et al. 2019) using the `DYNESTY` (Ashton & Talbot 2021) nested sampler. We assume a uniform prior for  $\tau$  and fixed  $t_0$ . For Gaussian pulse, we use the (flux-weighted) centroid of emission to define  $t_0$ . For a scattered pulse, we define  $t_0$  to be at leading edge at 10 per cent of the peak.

## 2.4 Maximizing S/N using match filtering

The weights calculated for individual time bins are used to average over frequency to generate coarser frequency channels as given by

$$P_{I,Q,U}(t, \nu) = \sum_{\nu=\nu_0}^{\nu_1} \sum_{t=0}^T S_{I,Q,U}(t, \nu) W_{\text{pulse}}(t), \quad (8)$$

where  $P_{I,Q,U}(t, \nu)$  are the on-pulse weighted average across frequency,  $S_{I,Q,U}(t, \nu)$  are the de-rotated Stokes I, Q, and U spectra and  $W_{\text{pulse}}(t)$  are the weights assigned to the individual sub-bursts for their respective time integrations. This is computed for all of the Stokes components, for both individual and integrated sub-bursts. The calculated linear polarization fractions from the coarser frequency channels are used in our modelling. We use a top-hat average for individual sub-bursts in the case of FRB 20190711A, due to its complex pulse morphology. The fractional linear polarization is calculated as  $L_{\text{de-bias}}/P_I$ , and the uncertainties in the  $L_{\text{de-bias}}$  are estimated using the uncertainties obtained in the Stokes I, Q, and U spectra ( $\sigma_I$ ,  $\sigma_Q$ , and  $\sigma_U$ , respectively) determined by

$$\sigma_L(\nu) = \left[ \left( \frac{P_U(\nu)}{\sqrt{P_Q^2 + P_U^2}} \sigma_U \right)^2 + \left( \frac{P_Q(\nu)}{\sqrt{P_Q^2 + P_U^2}} \sigma_Q \right)^2 \right]^{\frac{1}{2}}, \quad (9)$$

where  $P_{Q,U}$  is the weighted coarser sub-burst time-frequency averaged spectra and  $\sigma_{Q,U}$  is their respective uncertainties. The uncertainties in the original Stokes spectra are derived from their respective image-domain root-mean-square spectra, averaged using the weights derived from the pulse profiles for individual coarse channels. In the case of FRB 20191001A, we use the off pulse baseline to estimate these values. The uncertainty in the polarization fraction  $\sigma_{L/I}$  is calculated using

$$\sigma_{L/I}(\nu) = \frac{\sqrt{(\sigma_L^2 P_I^2 + L_{\text{de-bias}}^2 \sigma_I^2)}}{P_I^2}. \quad (10)$$

The uncertainties calculated from equation (10) are measured for individual sub-bursts across the averaged frequency channels. Further, likelihoods for individual models are generated using these estimates and compared individually.

## 2.5 Depolarization: comparison of models.

We consider two broad models for the observed linear polarization fraction of our FRB sample, with subcases for the depolarization model:

(1) Depolarization due to multipath propagation:

(a) Burn's law of foreground depolarization assuming 100 per cent intrinsic polarization at all frequencies (Burn 1966);

(b) Burn's law assuming a constant intrinsic fractional linear polarization at all frequencies that is < 100 per cent;

(2) Constant linear polarization fraction at all frequencies with no depolarization.

The linear polarization fraction calculated for the set of FRBs is independently fitted to all three models using a Bayesian framework. We perform an evidence comparison between the models using a Bayesian approach. We note that previous work only considered Case 1a (Feng et al. 2022).

Case 1a. *Burn's law of foreground depolarization*: In this case, the depolarization in frequency is entirely due to the scatter in RM

**Table 2.** Model comparison for the ASKAP FRB sample. Evidences are calculated for individual and integrated bursts. Higher values indicate preference for the model. For  $P_{\text{int}}$  68 per cent confidence intervals are reported, and for  $\sigma'_{\text{RM}}$  and  $\sigma_{\text{RM}}$ , 95 per cent CI upper limits are reported, except for FRB 20191001A. The scattering time-scales listed are from Bhandari et al. (2020), Day et al. (2020). The preferred model for each burst is shown in bold.

TNS	Sub-burst	Burn's law $\log_{10} B$	Const. polarization $\log_{10} B$	Mod. Burn's law $\log_{10} B$	$\sigma_{\text{RM}}$ $\text{rad m}^{-2}$	$\sigma'_{\text{RM}}$ $\text{rad m}^{-2}$	$P_{\text{int}}$	$\tau_s$ (ms)
FRB 20180924B	–	0.470	<b>0.88</b>	–0.16	<5.17	<4.01	$0.91^{+0.06}_{-0.07}$	$0.68^{+0.03}_{-0.03}$
FRB 20190102C	–	8.140	<b>9.43</b>	8.73	<5.52	<4.39	$0.84^{+0.05}_{-0.03}$	$0.041^{+0.002}_{-0.003}$
	sub-burst 0	– <b>1.07</b>	–1.42	–1.57	<9.85	<11.02	$0.74^{+0.17}_{-0.2}$	–
	sub-burst 1	8.19	<b>9.42</b>	8.74	<5.5	<4.33	$0.84^{+0.05}_{-0.03}$	–
FRB 20190608B	–	<b>1.85</b>	1.46	0.72	<5.42	<4.81	$0.93^{+0.05}_{-0.06}$	$3.3^{+0.2}_{-0.2}$
FRB 20190611B	–	2.95	<b>3.26</b>	2.60	<6.41	<5.48	$0.85^{+0.06}_{-0.04}$	$0.18^{+0.02}_{-0.02}$
	sub-burst 0	<b>3.61</b>	3.01	2.08	<3.58	<3.15	$0.97^{+0.02}_{-0.03}$	–
	sub-burst 1	2.62	<b>2.82</b>	2.41	<8.27	<7.28	$0.77^{+0.11}_{-0.06}$	–
FRB 20190711A	–	– <b>0.16</b>	–0.46	–1.04	<8.64	<8.93	$0.85^{+0.1}_{-0.2}$	–
	sub-burst 0	<b>0.84</b>	0.33	–0.44	<5.51	<5.09	$0.94^{+0.04}_{-0.07}$	–
	sub-burst 1	<b>0.53</b>	0.14	–0.63	<5.7	<5.18	$0.92^{+0.05}_{-0.09}$	–
	sub-burst 2	<b>0.01</b>	–0.28	–0.87	<7.92	<7.98	$0.86^{+0.1}_{-0.17}$	–
FRB 20191001A	–	4.82	<b>8.86</b>	7.89	$4.1^{+0.09}_{-0.10}$	<2.8	$0.6^{+0.06}_{-0.03}$	$3.3^{+0.2}_{-0.2}$

contributed by the line-of-sight (refer to Appendix A for discussion) and can be modelled as

$$P_{\text{Burn}}(\lambda) = \exp(-2\sigma_{\text{RM}}^2\lambda^4), \quad (11)$$

where  $P_{\text{Burn}}(\lambda)$  is the linear polarization fraction,  $\sigma_{\text{RM}}$  is the scatter RM, and  $\lambda$  is the wavelength of observation.

Case 1b. *Modified Burn's law*: Burn's law assumes 100 per cent polarization at infinite frequency. While many repeating FRBs show high degrees of linear polarization, this need not be the case. To model lower fractional linear polarization, we introduce  $P_{\text{int}}$ , which accounts for potentially lower polarization fraction, and a modified depolarization parameter  $\sigma'_{\text{RM}}$ :

$$P_{\text{modBurn}}(\lambda) = P_{\text{int}} \exp(-2\sigma'^2_{\text{RM}}\lambda^4). \quad (12)$$

Case 2. *Constant depolarization case*: We also consider the possibility that there is no foreground spectral depolarization and that depolarization is intrinsic to the source and constant across the band. In this case, the model is

$$P_{\text{no-depol}}(\lambda) = P_{\text{int}}, \quad (13)$$

where  $P_{\text{int}}$  parametrizes the depolarization.

The marginal likelihood is calculated for the models described above for each sub-burst as well as the total integrated burst. These are used to determine the Bayes factor and select a preferred model. Models 1a and 2 each have one parameter:  $\sigma_{\text{RM}}$  and  $P_{\text{int}}$ , respectively. For the modified Burn's law model, there are two parameters:  $P_{\text{int}}$  and  $\sigma'_{\text{RM}}$ . In all cases, we assume uniform priors on the parameters. For  $\sigma'_{\text{RM}}$  and  $\sigma_{\text{RM}}$ , we assume a uniform prior between 0 and 20  $\text{rad m}^{-2}$ . For  $P_{\text{int}}$ , we assume a uniform prior between 0 and 1.

### 3 RESULTS

The marginal likelihood for all the models is listed in Table 2, along with the maximum-likelihood parameters, the 95 per cent CI upper limits for  $\sigma'_{\text{RM}}$ , the  $1\sigma$  credible regions for  $P_{\text{int}}$  and  $\sigma_{\text{RM}}$ . We also

list the  $\tau_s$  measurements<sup>2</sup> reported in Bhandari et al. (2020) and Day et al. (2020) in Table 2. We report Bayes evidence ( $\log_{10} B$ ) for individual models and constraints on  $\sigma_{\text{RM}}$  and  $\sigma'_{\text{RM}}$  values for integrated bursts and sub-bursts in Table 2. We calculate three Bayes factors  $\Delta\log_{10} E_{\text{BL}}$ ,  $\Delta\log_{10} E_{\text{MD}}$ , and  $\Delta\log_{10} E_{\text{ND}}$ , for Case 1a–Case 2, Case 2–Case 1b, and Case 1a–Case 1b, respectively, to assess the pairwise preference of the models. To assess the significance of model preference, we follow Trotta (2008), interpreting  $\log_{10}$  evidence  $\Delta E \geq 10$  to be strong evidence and  $\Delta E \leq 1$  as inconclusive. We do this even when Burn's law and modified Burn's law are not favoured, as they can be used to constrain the magnetospheric properties of any foreground plasma.

With the exception of FRB 20191001A, which slightly favours the constant polarization model over Burn's depolarization model, the bursts in our sample do not show strong evidence for or against any of the models. The posterior probability distributions for all the models for FRB 20191001A are shown in Fig. 2. The preferred model fits for the linear polarization fraction for each FRB sub-burst and integrated burst are shown in Figs 3 and 4. While some of the components of some of the bursts show hints of depolarization (the first sub-burst of FRB 20190102C), the low S/N and fractional bandwidth results in inconclusive evidence.

## 4 DISCUSSION AND CONCLUSIONS

### 4.1 Depolarization in ASKAP bursts

We consider five non-repeating and one repeating FRB detected by ASKAP and place limits on both  $\sigma_{\text{RM}}$  and  $\sigma'_{\text{RM}}$  for each integrated burst and sub-burst (see Section 2.5 and Table 2). We use  $\sigma_{\text{RM}}$  for our further discussion, as  $\sigma'_{\text{RM}}$  conservatively accounts for potentially lower intrinsic linear polarization fraction.

<sup>2</sup>The measured  $\tau_s$  could have a systematic offset in case of an error in the DM measurement of the burst. For the bursts reported here, the  $\tau_s$  was modelled simultaneously with an additional parameter to account for any initial misestimation (Qiu et al. 2020).

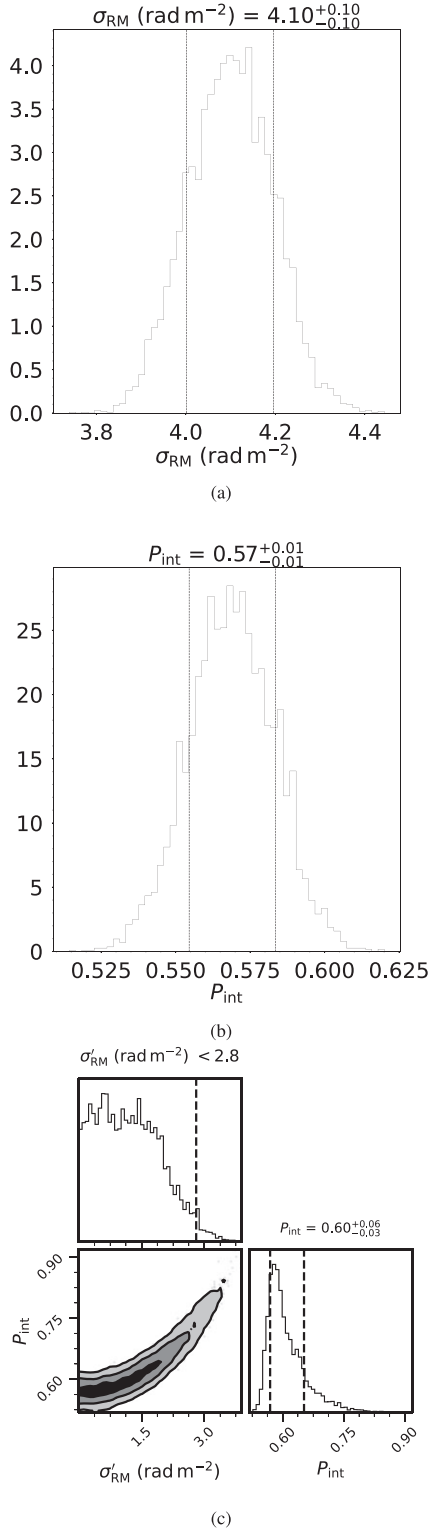


**Figure 2.** Posterior distributions for FRB 20191001A. We show the model for Burn’s law of foreground depolarization in panel (a), the constant polarization model in panel (b) and the modified version of the Burn’s law in panel (c). The dashed lines represent the 68 per cent uncertainty for panels (a) and (b). For panel (c), the dashed lines represent the 95 per cent upper limit for  $\sigma'_{RM}$  and 68 per cent uncertainty for  $P_{int}$ . The  $\sigma_{RM}$  derived from the unmodified Burn’s law (panel (a)) is disfavoured relative to the other two models shown in panels (b) and (c).

While we cannot determine conclusively whether or not the FRBs in our sample show spectral depolarization, we can place useful constraints on the presence of Burn’s depolarization and compare our limits to the measurements of  $\sigma_{RM}$  published in the literature (shown in Fig. 5). The upper limits on the derived  $\sigma'_{RM}$  are consistent with Feng et al. (2022)  $\sigma_{RM}$  and RM relationship, but not very constraining. The relationship between  $\sigma'_{RM}$  and RM is consistent only if the values of  $\sigma'_{RM}$  are  $\sim 2$  orders of magnitude smaller than our limits. If the model is applicable for non-repeating FRBs, then the depolarization would only be observable by ASKAP for events with orders of magnitude higher RM or (if non-repeating FRBs inhabit low-RM environments) detected with other instruments at lower frequencies. The latter would suggest environments that are much less magnetoionically complex.

Our upper limits on  $\sigma'_{RM}$ , however, are inconsistent with the relationship between  $\sigma'_{RM}$  and  $\tau_s$  observed in repeating FRBs.

This can be due to two scenarios:

(i) Even if a circumburst environment with similar properties to that inferred for repeating FRBs by Feng et al. (2022) exists, an additional source of scattering would be needed elsewhere along the line of sight. In this scenario, the scatter broadening could be attributed to the host-galaxy ISM and not the circumburst environment. This is in contrast to the repeating FRB sources, for which Feng et al. (2022) concluded that the temporal scattering and  $\sigma'_{RM}$  originated from the same inhomogeneous magnetoionic environment.

(ii) Alternatively, if a large fraction of scattering is being caused by the circumburst media, and not the host galaxy ISM, the inconsistency in the relationship between  $\sigma'_{RM}$  and  $\tau_s$  for repeating and non-repeating FRBs indicates a relatively less magnetized, but equally turbulent and dense, circumburst medium when compared with the repeating FRBs from Feng et al. (2022).

The relationship between temporal scattering and depolarization has been extensively studied in Yang et al. (2022) for various physical scenarios in repeating FRB sources. In the case of shock-compressed magnetized plasma Yang et al. (2022) predicts the  $\sigma_{RM} - \tau_s$  relationship to be  $\sigma_{RM} \propto \tau_s^{0.65-0.83}$ , which appears to be closer to the scaling index reported by Feng et al. (2022) for repeating sources. In general, the  $\sigma_{RM} - \tau_s$  scaling depends on various physical parameters, including the radius of the assumed turbulence scale  $R$  and  $B_{||}$ , with lower  $B_{||}$  leading to a shallower index of scaling or no correlation in  $\sigma_{RM} - \tau_s$ , which could be a characteristic of one-off FRBs. A similar correlation in the current set of one-off FRBs is not explored due to the lack of detection of depolarization in any non-repeating FRBs. To robustly test for a different relationship between  $\sigma_{RM}$  and RM for one-off bursts, FRBs with comparable RMs to that of repeating FRBs are essential, or the detection of depolarization (potentially using lower-frequency detection of one-off FRBs). The largest magnitude RM reported in a one-off FRB is only  $353 \text{ rad m}^{-2}$  for FRB 20190608B (Day et al. 2020).

Additionally, FRB 20190711A, which is a repeating FRB (Kumar et al. 2021), is consistent with the correlation model reported by Feng et al. (2022) if the  $\sigma'_{RM}$  is  $\sim 2$  orders of magnitude less than the reported upper limit. We do not plot the  $\sigma'_{RM}$  and  $\tau_s$  values of FRB 20190711A as no scattering time-scale measurements have been measured for this burst due to its complex burst morphology (in the case of the initial burst analysis in Day et al. 2020), and the low S/N of the repetition reported in Kumar et al. (2021). We also note that FRB 20190711A has been seen to repeat only once, even with an extensive follow-up campaign of  $\sim 293$  and  $\sim 19$  h



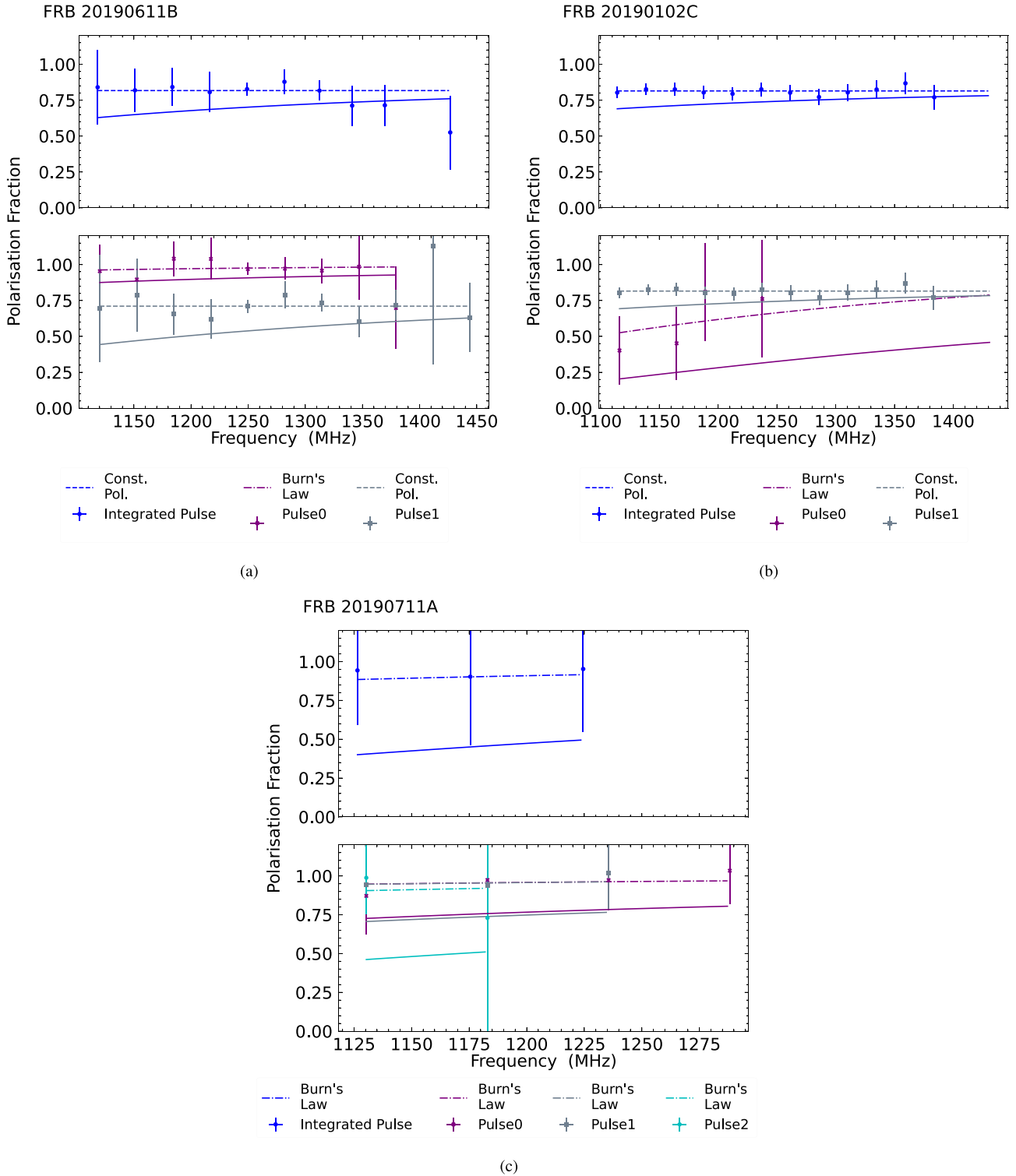


**Figure 3.** Fractional linear polarization of FRBs having multiple components (FRBs 20190611B, 20190102C, and 20190711A) across frequency. For each FRB, we show the model fit for the fractional linear polarization, which has the highest evidence in dashed lines. The top panel shows the linear polarization fraction for integrated pulse, and the bottom panel shows the linear polarization for each sub-pulse. The preferred model in each case is shown in Table 2. The solid lines denote the 95 per cent confidence upper limits derived from the modified Burn’s law for sub-bursts and integrated bursts. Some bursts (e.g. Pulse 0 in 20190611B, Pulse 0 in 20190102C) have polarization information in limited bandwidth due to lower polarized S/N, which are rejected due to de-biasing, hence polarization information in the higher frequency band is missing.

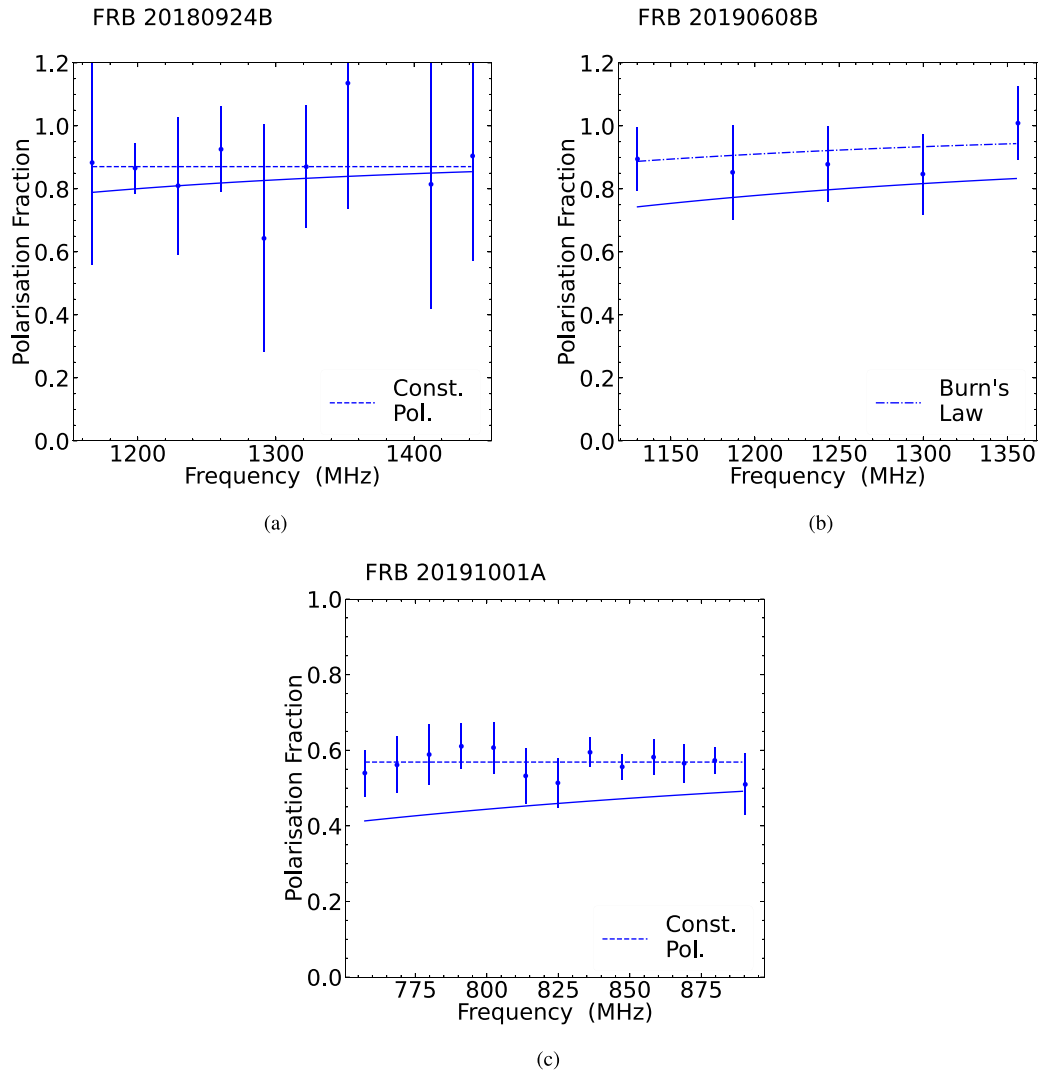


**Figure 4.** Fractional linear polarization of FRBs showing single components (FRBs 20180924B, 20190608B, and 20191001A) across frequency. The model fit for the fractional linear polarization having the highest evidence is shown in dashed lines. Table 2 shows the preferred model in each case. The solid lines denote the 95 per cent confidence upper limits derived from the modified Burn’s law for each FRB.

with ASKAP ICS and Parkes/Murriyang, respectively (Kumar et al. 2021).

The properties of host galaxies of localized repeating and (apparently) non-repeating FRB sources do not show a strong distinction in global properties (Bhandari et al. 2022). This provides potential evidence that we might expect similar lines of sight through bulk interstellar media, hence comparable ionized ISM for both the samples. As such, we might expect similar  $\tau_s$  for both repeating and non-repeating FRBs but the  $\sigma'_{RM}$  to be independent and likely caused due to local environment. In this case, we would not expect there to be a positive correlation between  $\tau_s$  and  $\sigma'_{RM}$  for non-repeaters, as observed in repeating FRBs. Further, Fig. 6, which shows the relationship between RM and  $\tau_s$ , suggests similar  $\tau_s$  but lower RMs for non-repeaters, which supports the scenario of less magnetized environments for non-repeaters. However, we caution the reader that a more extensive sample set of non-repeaters with polarization measurements are required to confirm this.

While the differences in circumburst environments could be the result of non-repeating and repeating FRBs having different

progenitors (e.g. Caleb et al. 2019; Cui et al. 2021), it is also possible that they have the same progenitor, with non-repeating FRBs sourced by an older population that has become less magnetoionically active in the later stages of its evolution.

Furthermore, for repeating FRBs such as FRBs 20201124A and 20190520B, depolarization and RM variation have been speculated to be due to a magnetar main sequence Be-type star binary system, containing a decretion disc (Anna-Thomas et al. 2022; Wang et al. 2022), similar to the B1259-63 system (Johnston et al. 1996). However, in the case of non-repeating FRBs, since the follow-up observations are inherently unachievable, it necessitates future wide-band polarimetric observations to correctly characterize the depolarization from a single burst and rule out possible progenitor models based on depolarization characteristics.

#### 4.2 Effect of bandwidth in model selection

The combination of the bandwidth of the instrument, observing frequency, and the S/N of the burst can impact our ability to

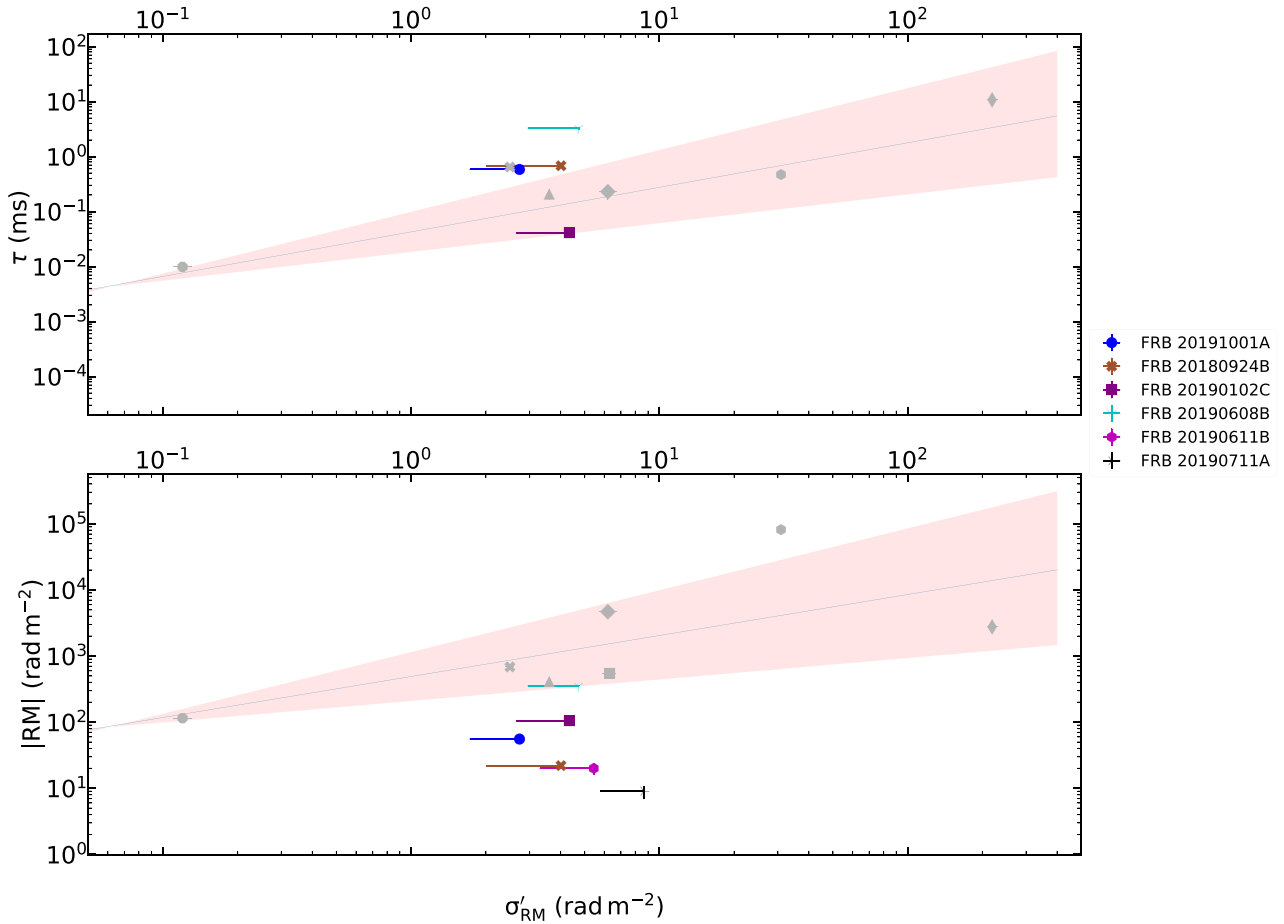


**Figure 5.** Comparison of  $\sigma'_{\text{RM}}$ , pulse broadening, and RM. The conservative  $\sigma'_{\text{RM}}$ , 95 per cent confidence upper limits are derived from fitting the polarization profiles of the individual bursts with modified Burn’s law. The grey points are previously reported repeating FRBs. The scattering times for all the bursts have been scaled to 1271 MHz, assuming a  $\nu^{-4}$  dependence of scattering time-scale. The blue lines are the correlation fit previously reported in Feng et al. (2022). The red region indicates the  $1\sigma$  uncertainty on the linear model from Feng et al. (2022). The uncertainties in RM are too small to see by eye.

constrain spectral depolarization. While this is more pronounced in the case of repeating FRBs, which tend to be band-limited in comparison to that of one-off FRBs (Pleunis et al. 2021b), by using follow-up observations at different frequencies, the polarization properties can be measured over a range of frequencies, leading to a robust selection of a depolarization model and an estimate of  $\sigma'_{\text{RM}}$ . This is difficult for a one-off FRB with a limited instrumental bandwidth. In the case of ASKAP non-repeating FRBs, a maximum of 336 MHz of the spectral window is achievable. However, even with this limited bandwidth, a better estimation of the parameters and the model is possible with bursts for which rapid exponential suppression of linear polarization occurs within the band. For ASKAP, assuming 1271 and 824 MHz as the central frequencies, and a 100 per cent intrinsic polarization fraction, it will be most sensitive to a  $\sigma'_{\text{RM}}$  of 12.68 and 5.35  $\text{rad m}^{-2}$ , respectively.

The ability to measure  $\sigma_{\text{RM}}$  depends on the S/N ratio of the burst. With a burst of S/N 61 (e.g. the highest S/N burst in our sample, reported by FRB 20191001A (Bhandari et al. 2020)), which corresponds to an uncertainty of 30 per cent in the linear

polarization fraction within a 1 MHz channel, over a bandwidth of 336 MHz and a centre frequency of 824 MHz, no model discrimination would be possible above  $\sigma'_{\text{RM}}$  of 8  $\text{rad m}^{-2}$ , and below 4  $\text{rad m}^{-2}$ . Additionally, a broad-band burst detected by the Ultra Wideband Low (UWL) receiver on Parkes (Hobbs et al. 2020) with an uncertainty of 10 per cent in linear polarization, for an RM-corrected<sup>3</sup> 128 MHz sub-band in 3328 MHz of bandwidth, and a corresponding burst S/N of 55 should be able to discriminate depolarization models across  $\sigma'_{\text{RM}}$  of 3 and 81  $\text{rad m}^{-2}$ . Thus, future wide-band polarimetric depolarization studies, or multifrequency simultaneous detection of bursts from different instruments, are required to better model the depolarization behaviour, especially for non-repeaters.

<sup>3</sup>Rate in full Stokes data mode providing a typical spectral resolution of 0.5 MHz. We assume here that we correct for RM before averaging the finer channels together. We choose 10 per cent uncertainty and 128 MHz as the channel width to realistically model a potential burst to have a total polarized SNR of 55.

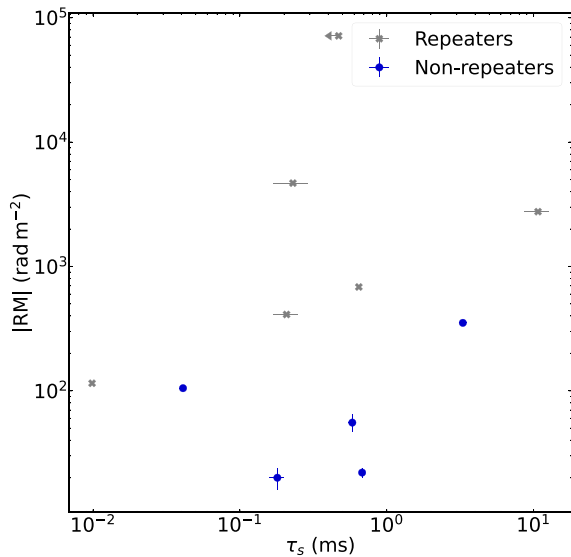


**Figure 6.** RM– $\tau_s$  relationship for repeaters reported in Feng et al. (2022), and our sample of non-repeaters. The  $\tau_s$  for both repeaters and non-repeaters have been scaled to 1271 MHz, assuming a  $\nu^{-4}$  dependence of the scattering time-scale. The non-repeating FRB sample clearly shows a lower RM than that of the repeating FRBs for any given  $\tau_s$ .

## ACKNOWLEDGEMENTS

PAU and RMS acknowledges support through Australia Research Council Future Fellowship FT190100155. RMS and ATD acknowledge support through Australian Research Council Discovery Project DP220102305. KG and ATD acknowledge support through DP200102243. SB is supported by a Dutch Research Council (NWO) Veni Fellowship (VI.Veni.212.058). This scientific work uses data obtained from Inyarrimanha Ilgari Bundara / the Murchison Radio-astronomy Observatory. We acknowledge the Wajarri Yamaji People as the Traditional Owners and native title holders of the Observatory site. The Australian SKA Pathfinder is part of the Australia Telescope National Facility (<https://ror.org/05qajvd42>), which is managed by CSIRO. Operation of ASKAP is funded by the Australian Government with support from the National Collaborative Research Infrastructure Strategy. ASKAP uses the resources of the Pawsey Supercomputing Centre. Establishment of ASKAP, the Murchison Radio-astronomy Observatory, and the Pawsey Supercomputing Centre are initiatives of the Australian Government, with support from the Government of Western Australia and the Science and Industry Endowment Fund.

This work makes use of BILBY (Ashton et al. 2019), MATPLOTLIB (Hunter 2007), and NUMPY (Harris et al. 2020) software packages.

## DATA AVAILABILITY

No new data were generated in this work.

## REFERENCES

- Anna-Thomas R. et al., 2022, *Science*, 380, 599  
 Ashton G., Talbot C., 2021, *MNRAS*, 507, 2037  
 Ashton G. et al., 2019, *ApJS*, 241, 27  
 Bannister K. W. et al., 2019, *Science*, 365, 565

- Bethupudi S., Spitler L. G., Main R. A., Li D. Z., Wharton R. S., 2022, *MNRAS*, 524, 3303  
 Bhandari S. et al., 2020, *ApJ*, 901, L20  
 Bhandari S. et al., 2022, *AJ*, 163, 69  
 Burn B. J., 1966, *MNRAS*, 133, 67  
 Caleb M., Stappers B. W., Rajwade K., Flynn C., 2019, *MNRAS*, 484, 5500  
 Chatterjee S. et al., 2017, *Nature*, 541, 58  
 CHIME/FRB Collaboration et al., 2019, *Nature*, 566, 235  
 Chime/FRB Collaboration et al., 2020, *Nature*, 582, 351  
 CHIME/FRB Collaboration et al., 2021, *ApJS*, 257, 59  
 Cho H. et al., 2020, *ApJ*, 891, L38  
 Cui X.-H. et al., 2021, *MNRAS*, 500, 3275  
 Day C. K. et al., 2020, *MNRAS*, 497, 3335  
 Everett J. E., Weisberg J. M., 2001, *ApJ*, 553, 341  
 Feng Y. et al., 2022, *Science*, 375, 1266  
 Gajjar V. et al., 2018, *ApJ*, 863, 2  
 Gardner F. F., Whiteoak J. B., 1963, *Nature*, 197, 1162  
 Gourdji K., Michilli D., Spitler L. G., Hessels J. W. T., Seymour A., Cordes J. M., Chatterjee S., 2019, *ApJ*, 877, L19  
 Harris C. R. et al., 2020, *Nature*, 585, 357  
 Hessels J. W. T. et al., 2019, *ApJ*, 876, L23  
 Hilmarsson G. H. et al., 2021, *ApJ*, 908, L10  
 Hobbs G. et al., 2020, *PASA*, 37, e012  
 Hunter J. D., 2007, *Comput. Sci. Eng.*, 9, 90  
 James C. W. et al., 2022, *MNRAS*, 516, 4862  
 Johnston S., Manchester R. N., Lyne A. G., D’Amico N., Bailes M., Gaensler B. M., Nicastro L., 1996, *MNRAS*, 279, 1026  
 Kumar P. et al., 2021, *MNRAS*, 500, 2525  
 Kumar P., Shannon R. M., Lower M. E., Bhandari S., Deller A. T., Flynn C., Keane E. F., 2022, *MNRAS*, 512, 3400  
 Le Roux E., 1961, *ANAP*, 24, 71  
 Lorimer D. R., Bailes M., McLaughlin M. A., Narkevic D. J., Crawford F., 2007, *Science*, 318, 777  
 Luo R. et al., 2020, *Nature*, 586, 693  
 Macquart J. P. et al., 2020, *Nature*, 581, 391  
 Mannings A. G. et al., 2022, *ApJ*, 954, 179  
 Michilli D. et al., 2018, *Nature*, 553, 182  
 Niu C. H. et al., 2022, *Nature*, 606, 873  
 Pleunis Z. et al., 2021a, *ApJ*, 911, L3  
 Pleunis Z. et al., 2021b, *ApJ*, 923, 1  
 Prochaska J. X. et al., 2019, *Science*, 366, 231  
 Qiu H. et al., 2020, *MNRAS*, 497, 1382  
 Rajwade K. M. et al., 2020, *MNRAS*, 495, 3551  
 Ravi V., 2019, *Nat. Astron.*, 3, 928  
 Spitler L. G. et al., 2016, *Nature*, 531, 202  
 Thornton D. et al., 2013, *Science*, 341, 53  
 Trotta R., 2008, *Contemp. Phys.*, 49, 71  
 Wang F. Y., Zhang G. Q., Dai Z. G., Cheng K. S., 2022, *Nat. Commun.*, 13, 4382  
 Wardle J. F. C., Kronberg P. P., 1974, *ApJ*, 194, 249  
 Xu J. et al., 2023, *Universe*, 9, 330  
 Yang Y.-P., Lu W., Feng Y., Zhang B., Li D., 2022, *ApJ*, 928, L16

## APPENDIX A: BURN’S DEPOLARIZATION MODEL

The Faraday Dispersion Function described in Burn (1966) relates the complex linear polarization function  $P(\lambda^2)$  to a Faraday dispersion function (FDF,  $F(\phi)$ ) using a Fourier transform. It describes the polarization behaviour of the source across wavelength due to the Faraday dispersion caused by the intervening media. It can explain the decrease in observed polarization fraction in wavelength for sources which are expected to have a polarization fraction independent of frequency (Le Roux 1961). The FDF relates the



complex polarized brightness of the source at unit Faraday depth  $\phi$ :

$$P(\lambda^2) = \int_{-\infty}^{\infty} F(\phi) \exp(2i\phi\lambda^2) d\phi, \quad (\text{A1})$$

where  $P(\lambda^2) = Q(\lambda^2) + iU(\lambda^2)$  is the complex polarization function and  $\lambda$  is the wavelength.  $\phi(r)$  is the Faraday depth of the emission:

$$\phi(r) = 0.81 \int_r^0 n_e \mathbf{B} \cdot d\mathbf{r}, \quad (\text{A2})$$

where  $n_e$  is the electron density in  $\text{cm}^{-3}$ ,  $B$  is the magnetic field in  $\mu\text{G}$  and  $dr$  is the infinitesimal path length in parsec. In this case, the units of  $\phi(r)$  are  $\text{rad m}^{-2}$ . Depolarization can also arise due to beam depolarization. However, this is not applicable to FRBs, which are point sources relative to the beam of the telescope. Using equation (A1), the FDF can be calculated assuming  $P(\lambda^2)$  to be Hermitian, which was successfully demonstrated for early observations of Crab nebula (Gardner & Whiteoak 1963; Burn 1966). There are two possible sources for depolarization, internal and external to the emission region. Any change in the sign or strength of the parallel component of the magnetic field across the source emission region will lead

to depolarization, as the emission will arise from different rotation measures. This is less likely to be the case for FRBs, as the emission is constrained to come from a region smaller than  $300 \text{ km } \Gamma w_{i,-3}$ , where  $w_{i,-3}$  is the intrinsic burst width measured in ms, and  $\Gamma$  is the (currently theoretically unconstrained) Lorentz factor of the source plasma. The emitting region is also likely to reside in a relativistic plasma, which does result in conventional Faraday rotation.

The second component of the depolarization relates to the foreground turbulent RM scatter, which is separate from the internal depolarization. Considering the distribution of RM as a Gaussian random variable, the expectation of equation (A1) results in equation (11).

A final contribution to depolarization could be due to the polarized foreground emission. In our analysis, the polarized emission from a constant foreground is removed during the off-pulse subtraction of the Stokes spectrum.

This paper has been typeset from a  $\text{\TeX/L\AA\TeX}$  file prepared by the author.